DOI: 10.61782/fa.2025.0554

FORUM ACUSTICUM EURONOISE 2025

MEASURES OF VALIDATION FOR COMPUTATIONAL ROOM ACOUSTICS

Albert G. Prinn[1*] **Zeyu Xu**[2] **Emanuël A. P. Habets**[2]
[1] Fraunhofer Institute for Integrated Circuits (IIS), Erlangen, Germany
[2] International Audio Laboratories Erlangen[†], Germany
[†]A joint institution of the Friedrich-Alexander-Universität Erlangen-Nürnberg (FAU) and Fraunhofer Institute for Integrated Circuits (IIS)

ABSTRACT

Recent advances in computational methods and machine learning have spurred the development of new room acoustic modeling methods. For instance, some models leverage discontinuous Galerkin methods on GPU clusters, while others, currently evolving in various research labs, employ generative deep learning. As these innovations bring us closer to accurately simulating room acoustics across the entire audible frequency range, it is crucial to ensure their reliability. This paper examines what constitutes a trustworthy solution in room acoustics simulation. By analyzing the features of room transfer functions, room impulse responses, and energy decay curves through simulation-based parameter studies and fundamental physical principles, we propose a set of advisory measures to assess the accuracy of simulated room acoustics against measured data.

Keywords: *Computational modeling, Room acoustics, Measures of validation.*

1. INTRODUCTION

A wide range of computational methods for simulating room acoustics can be found in the literature and industry. A distinction is often made between wave and geometrical modeling methods. While wave models tend to be more accurate, geometrical models are used more frequently due to their efficiency. In the pursuit of more efficient methods, the room acoustics community has recently started experimenting with machine learning models. With the rise of machine learning methods, the accuracy of simulated data has become a pertinent issue. The reason is that it is difficult to train a machine-learning model using only measured data, due to its scarcity, and simulated data is often used to augment available measured data. Using inaccurate simulated data has the potential to generate low-quality machine learning models, which, while efficient, may be highly inaccurate. Thus, there is a need to determine the accuracy of computational methods used to generate room acoustics data. Additionally, there is a need to confirm that the outputs of machine learning models adequately reflect the physical system being modeled. Therefore, this work aims to provide users of room acoustics simulation tools with a set of measures for estimating the accuracy of the tool at hand.

This paper is organized as follows: Section 2 reviews the literature related to the validation of computational methods room acoustics simulations. Section 3 presents a parameter study using Finite Element Method (FEM) and Image Source Method (ISM) models. In Sec. 4, a preliminary set of validity measures based on the study's observations are proposed and subsequently used to assess FEM and ISM models of a measured shoebox-shaped room in Sec. 5. Finally, conclusions are drawn in Sec. 6.

2. LITERATURE REVIEW

We define verification as the process of ensuring that a simulation tool's output aligns with the mathematical model it aims to solve, while validation confirms that the output matches data from the physical world. This work

***Corresponding author**: *albert.prinn@iis.fraunhofer.de.*

focuses solely on validation, i.e., comparing measured and simulated data. Although the topic of model validation has a rich history, this literature review intends to cover only the basics without being exhaustive.

Russel [1] introduces magnitude and phase error measures for two transient signals and provides a single metric to assess simulated transient response accuracy. His phase error metric is based on cosine similarity. Schwer [2] reviews two alternative validation metrics for waveforms and highlights the role of expert opinion in validation. Roy and Oberkampf [3] present a framework for verification, validation, and uncertainty quantification in scientific computing, defining validation metrics as mathematical operators that quantify simulation uncertainty.

Vorländer [4] highlights the uncertainties in geometrical acoustic models and emphasizes the need for reliable input data. Aspöck [5] analyzes the validity of geometrical acoustic simulations and shares a measurement database [6] to facilitate comparisons. Aspöck highlights the need for reliable input data to describe boundary conditions in validating a suite of available geometrical models.

Thydal *et al.* [7] examine the validation of wave models, focusing on uncertainties in room parameters like reverberation time and clarity. Their research targets the discontinuous Galerkin method and uses just noticeable differences to measure perceptual validity. The results indicate that the uncertainty in the input data is too high for the model's errors to remain below the just noticeable difference threshold.

This study explores the performance of wave and geometrical models from a deterministic perspective. Measures of validation in both the time and frequency domains are proposed.

3. PARAMETER STUDY

A parameter study is carried out to assess the influence of varying room parameters on Room Impulse Responses (RIRs), Energy Decay Curves (EDCs), and Room Transfer Functions (RTFs). A simple test case is used to analyze both the FEM and the ISM. As both methods are deterministic, their solutions enable us to evaluate the effects of parameter changes on the acoustic field, aiding in the development of validation measures.

3.1 Test case

The chosen test case is a shoebox-shaped room with nominal dimensions $V = 4.0 \times 3.0 \times 2.5$ m^3. The air within the room has a density of 1.2 kg/m^3 and a nominal speed of sound of $c_0 = 343$ m/s. The room's acoustic field is excited by a point source, located at (1.0,1.0,1.0) m, and is observed at a point receiver, located at (3.0,2.0,1.5) m. A point source is used since it can be difficult to accurately describe a source of finite extent in the standard ISM. Additionally, the point source and receiver are placed away from the walls to minimize the error incurred by the ISM.

Two absorbing surfaces are considered. The first is a constant real-valued normalized impedance of 32.56, which is equivalent to a random incidence absorption coefficient of 0.2. This impedance is applied to the floor and walls. The second is a porous material fixed to the ceiling. The porous material is modeled using the Delany-Bazley-Miki model [8], with a depth of 10 cm, and a nominal flow resistivity of $\sigma_0 = 2 \times 10^4$ Pa.s/m^2. Consequently, the impedance of the room's surfaces is spatially non-uniform, complex-valued, and frequency-dependent.

With this model, we can vary the speed of sound, the room volume, and the flow resistivity of the porous material impedance model. While other parameters could be varied, for brevity, we consider only these three [1]. We observe the changes in both the time domain and frequency domain solutions.

3.2 Computational models

FEM and ISM models of the test case are used for the parameter study. Adequately resolved models are used (details are given below). Solutions are obtained in the frequency domain due to the consideration of frequency-dependent boundary conditions, and inverse Fourier transformation is applied to derive the time domain solutions.

The source signal used is a Ricker wavelet with unit amplitude, a center frequency of 140 Hz, and a delay of 0.05 s. The signal is generated using a sample frequency of 1 kHz, and a period of $T = 0.4$ s. The signal is Fourier transformed, and the resulting frequency vector and Fourier coefficients are used to define the source condition. This signal and these parameters are chosen to minimize the errors associated with the inverse Fourier Transform's wrap-around effect (see, e.g., Prinn [9]).

3.2.1 Finite element model

The commercial code COMSOL [10] is used to generate FEM solutions for the test case. It is expected that this

[1] Thus, we fix the source and receiver positions and the source signal. Studies of the effect of these and other model input parameters are left for future work.

code is free from implementation errors. To ensure that the model is sufficiently resolved, quintic elements with 7 degrees of freedom per wavelength at 500 Hz are used.

3.2.2 *Image source model*

An in-house ISM code is used. The boundary conditions are defined using angle-dependent reflection coefficients (see, e.g., Suh and Nelson [11]) computed from the surface impedances. To ensure that the reverberant tail of the RIR is captured down to -60 dB, the maximum reflection orders used for each dimension are

$$[N_x, N_y, N_z] = \text{round}\left(\frac{c_0 T}{2 \times [4, 3, 2.5]}\right) = [17, 23, 27] .$$

3.3 Speed of sound

We vary the nominal speed of sound by $\pm 2\%$. This is similar to varying the temperature in the room by approximately $\pm 10°$C. In Fig. 1a, the RIRs of the FEM and ISM solutions are compared for the three speeds of sound. As expected, the arrival times of peaks in the RIRs vary with the speed of sound. For lower speeds, the peaks arrive at later times. The RIRs of the two modeling methods appear to be similar. The EDCs are compared in Fig. 1b. The differences caused by varying the speed of sound are smaller than the differences between the modeling methods. The reason for this becomes clear upon consultation of the RTFs shown in Figs. 1c and 1d. The resonance peaks of the FEM RTFs have higher Q-factors than those of the ISM RTFs. Considering the varying speed of sound, a lower speed of sound results in resonance peaks with lower frequencies.

3.4 Room volume

The room has one corner at the origin of a Cartesian coordinate system. The room's volume is varied by $\pm 10\%$. The room's dimensions are shortened or lengthened, while the source and receiver positions remain fixed relative to the origin. The resulting solutions are shown in Fig. 2. We see that changing the room's volume has the opposite effect on the RIRs and RTFs to changing the speed of sound. For a smaller room, the peaks in the RIRs arrive earlier, and the resonance peaks in the RTFs appear at higher frequencies. Once again, the difference between the EDCs of the two modeling methods is larger than the differences that appear when varying the room volume.

3.5 Flow resistivity

The nominal flow resistivity is varied by orders of magnitude, i.e., $[\sigma_{-1}, \sigma_0, \sigma_{+1}] = [2 \times 10^3, 2 \times 10^4, 2 \times 10^5]$ Pa.s/m^2. The solutions obtained are shown in Fig. 3. The RIRs, given in Fig. 3a, appear to show that varying the flow resistivity does not change the arrival times of the peaks. The amplitudes of the peaks, however, are changed. This can be seen in more detail in the EDCs shown in Fig. 3b. It is to be expected that varying the flow resistivity affects the energy decay since the absorption of the room's ceiling is being varied. The RTFs given in Figs. 3c and 3d, show that the resonance peaks appear at similar frequencies for each instance of the flow resistivity. However, the Q-factors and amplitudes of the resonance peaks vary noticeably. This is due to the frequency-dependency of the complex-valued impedance model used, which varies with flow resistivity.

3.6 Summary

Varying the speed of sound and room volume (and, thus, geometry) affects the positions of the peaks in the RIRs and RTFs. It also affects the decaying energy. Varying the impedance affects the amplitudes of the peaks in the RIRs, the decay rate of the energy, and the Q-factors and amplitudes of the peaks in the RTFs. [2] Thus, the peaks in the RIRs and RTFs can be associated with the medium and geometry parameters, while the EDCs and Q-factors of the RTFs can be associated with the room's sound absorption.

4. PROPOSED VALIDATION MEASURES

Information contained within the RIRs and RTFs can be used to validate a room model. For example, if the model's solution captures the effect of the room's geometry, then the peaks in the RIRs and RTFs should agree with measured data, or if the sound absorption is accurately described by the model, then the simulated energy decay should agree with measured energy decay. Therefore, instead of computing an absolute or relative error for the entire simulation solution, which will be adversely affected by noise and uncertainty, we define measures that consider specific features of the acoustic field. We expect that if sufficiently minor errors are found for these features, a model is a valid representation of the physical system, at least with respect to those features. In the following, we consider six measures.

[2] Note that varying the impedance can also affect the resonance frequencies.

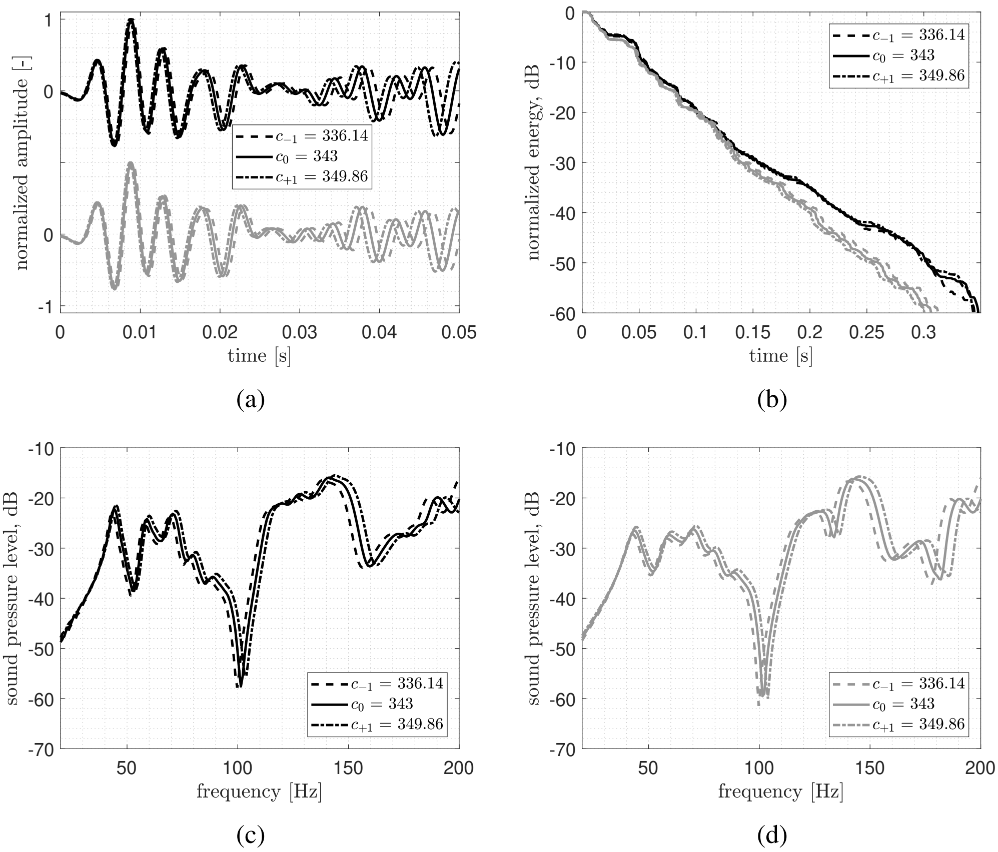

Figure 1: Varying speed of sound. FEM data are shown using black lines, and ISM data are shown using gray lines. (a) RIRs. (b) EDCs. (c) FEM RTFs. (d) ISM RTFs. RIRs, EDCs normalized by max., RTFs by L_2 norm.

4.1 Time domain

Three measures are used to compare the measured and simulated RIRs. The first is a cosine similarity measure, the second measure compares the RIRs at the peak arrival times only, and the third measure compares the EDCs of the RIRs.

4.1.1 Cosine similarity relative error

It can be difficult to extract useful information from a direct comparison, using, for example, the Euclidean norm, of the measured and simulated data due to uncertain level offsets that might be present in the data. A possible alternative is to use the cosine similarity of the measured and simulated RIRs, similar to the phase error metric considered by Russel [1]. The cosine similarity compares the gain invariant features of two vectors, which is interesting for our study. The cosine similarity used here is written

$$S_{\mathrm{t}} = \frac{\mathbf{h}_{\mathrm{m}} \cdot \mathbf{h}_{\mathrm{s}}}{||\mathbf{h}_{\mathrm{m}}||_2 ||\mathbf{h}_{\mathrm{s}}||_2} , \tag{1}$$

where $\mathbf{h}_{\mathrm{m}}$ is the measured RIR at some receiver position, $\mathbf{h}_{\mathrm{s}}$ is the simulated RIR at the same position, and $\|\cdot\|_2$ is the L_2 norm. If the features of two normalized RIRs are identical, then $S_f = 1$. If there is no agreement, then $S_f = 0$. If the normalized RIRs are identical but out of phase, then $S_f = -1$. Writing the cosine similarity in terms of a signed relative error, we obtain

$$E_{S_{\mathrm{t}}} = \mathrm{sign}(S_{\mathrm{t}})(1 - |S_{\mathrm{t}}|) \times 100 , \tag{2}$$

where the sign indicates whether or not the RIRs are in phase. This measure reports the relative similarity of measured and simulated RIRs. Since the disagreement

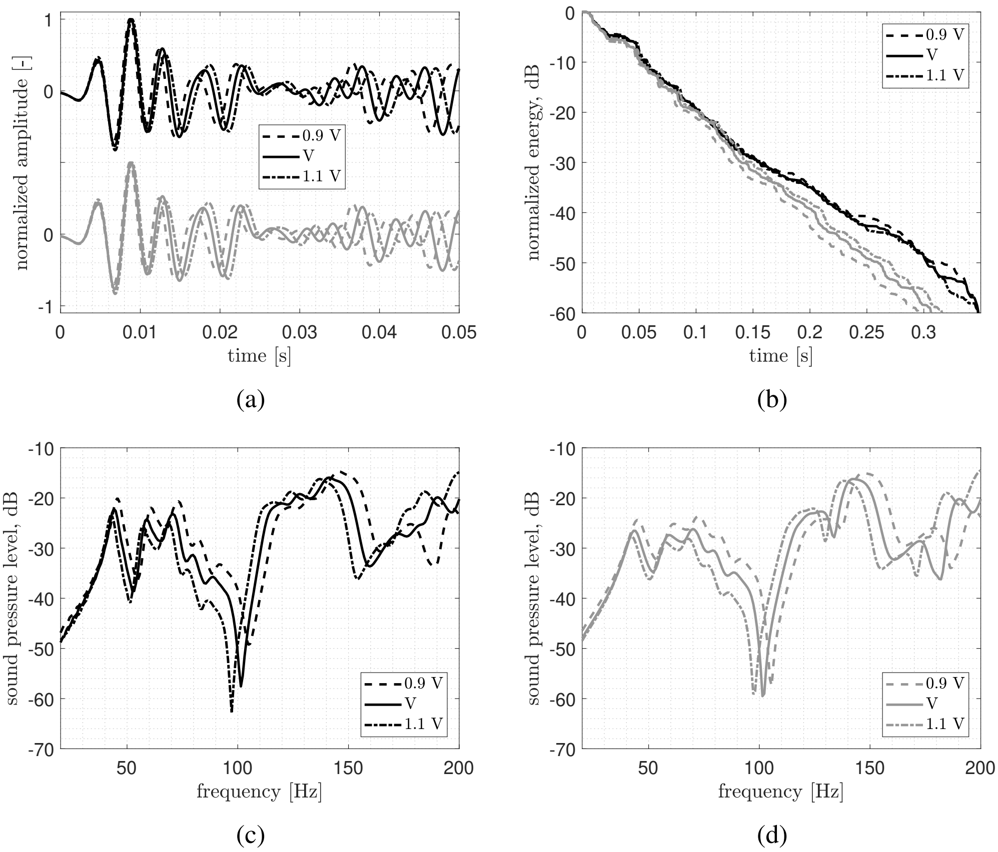

Figure 2: Varying room volume. FEM data are shown using black lines, and ISM data are shown using gray lines. (a) RIRs. (b) EDCs. (c) FEM RTFs. (d) ISM RTFs. RIRs, EDCs normalized by max., RTFs by L_2 norm.

between the two RIRs will probably increase with time, choosing a limited range of time values for this measure can be beneficial. Choosing the early part of RIRs indicates the ability of the model to capture medium and geometry effects (since these affect peak arrival times).

4.1.2 Peak arrival time error

For the second measure, we use a peak-finding algorithm to identify the arrival times of the peaks in both datasets. Since the peak arrival times might not agree, we use the peaks of one dataset as a reference set and find the closest peaks from the other dataset. Since the simulated data is likely to be noise-free, we use the set of simulated peak arrival times as the reference set. The relative error of each peak arrival time can be computed and presented as a function of the reference arrival times. However, for simplicity, the measure proposed here is the mean relative error of the peak arrival times. The measure is

$$E_{p_t} = \frac{1}{N}\sum_{n=0}^{N}\frac{|\tau_{\mathrm{m},n} - \tau_{\mathrm{s},n}|}{\tau_{\mathrm{m},n}} \times 100\,, \tag{3}$$

where $\tau_{\mathrm{m},n}$ is the nth time of arrival of the measured data, and $\tau_{\mathrm{s},n}$ is the nth time of arrival of the simulated data.

4.1.3 Reverberation time error

A straight line is fitted to the EDCs for a range of decay values. The offset of the straight line is removed, and the time at which the straight line reaches -60 dB is used to estimate the reverberation time. The relative error of the reverberation times can then be computed. This measure could be computed for a range of frequencies, e.g., third-octave band center frequencies. For simplicity, a single reverberation time is found for each RIR in this work. The

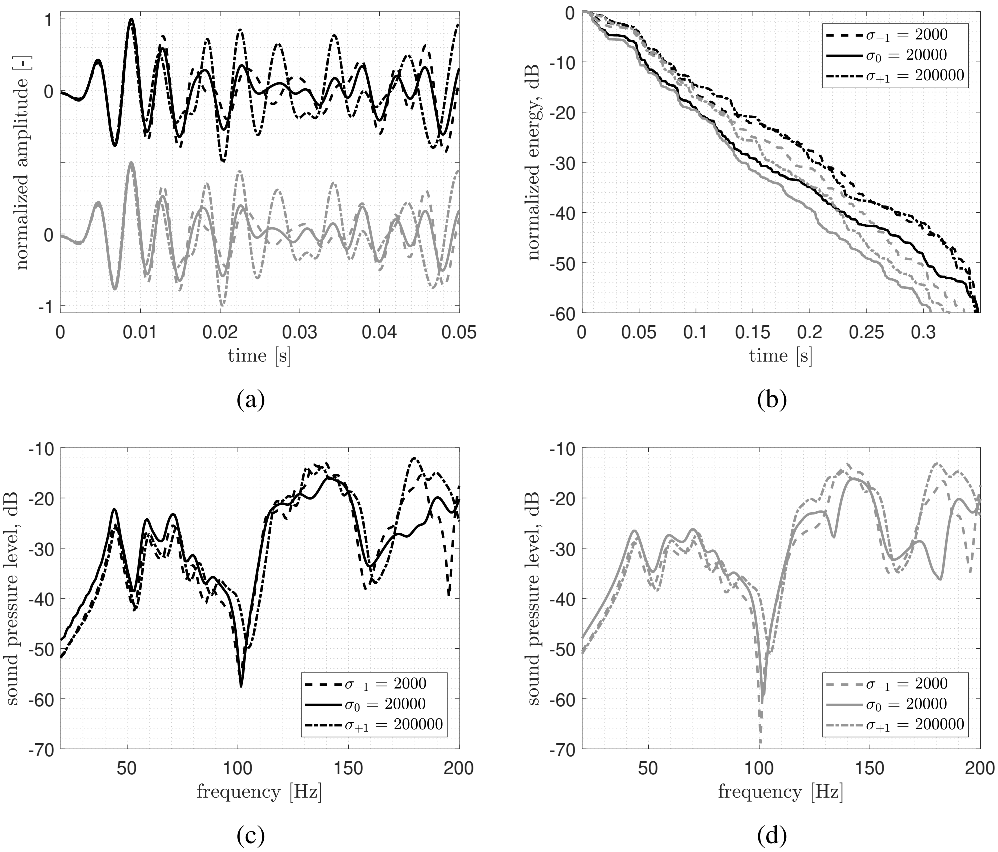

Figure 3: Varying flow resistivity. FEM data are shown using black lines, and ISM data are shown using gray lines. (a) RIRs. (b) EDCs. (c) FEM RTFs. (d) ISM RTFs. RIRs, EDCs normalized by max., RTFs by L_2 norm.

reverberation time error is given by

$$E_{T_{60}} = \frac{|T_{60,\text{m}} - T_{60,\text{s}}|}{T_{60,\text{m}}} \times 100 \,, \tag{4}$$

where $T_{60,\text{m}}$ is the estimated reverberation time of the measured data, and $T_{60,\text{s}}$ is the reverberation time of the simulated data.

4.2 Frequency domain

In the frequency domain, we consider the cosine similarity, the frequencies of resonance peaks in the RTFs, and a representation of the damping of room modes.

4.2.1 Cosine similarity relative error

By comparing normalized RTFs, the similarity of the spectral envelope rather than the magnitude is emphasized, which provides a useful measure of the features of the RTFs. The cosine similarity is given by

$$S_\text{f} = \frac{\mathbf{H}_\text{m}^* \cdot \mathbf{H}_\text{s}}{||\mathbf{H}_\text{m}||_2 ||\mathbf{H}_\text{s}||_2} \,, \tag{5}$$

where $\mathbf{H}_\text{m}$ is the RTF measured at a position, $\mathbf{H}_\text{s}$ is the simulated RTF at the same position, and $(\cdot)^*$ is the complex conjugate. We use this as a measure of the agreement between the normalized RTFs, as follows:

$$E_{S_\text{f}} = \text{sign}(\text{Re}(S_\text{f}))(1 - |S_\text{f}|) \times 100 \,. \tag{6}$$

This measure estimates the relative error between the normalized RTFs, and the sign of the error provides information on the phase between the corresponding RIRs. It can be insightful to limit the spectrum range used for this measure. Limiting the range to modal frequencies has the benefit of quantifying the ability of the model to capture the effect of the medium and the room's geometry.

4.2.2 Resonance frequency error

For this measure, we use a peak-finding algorithm to identify the peaks in both data sets and subsequently determine the frequencies at which these peaks occur. Since the measured data contains noise while the simulated data does not, it is more convenient to select a peak from the simulated transfer function and search for the closest match in the measured transfer function. The error can then be computed for each resonance frequency. However, for simplicity, a mean error is calculated here. The relative error is calculated as follows

$$E_{p_\mathrm{f}} = \frac{1}{N}\sum_{n=0}^{N} \frac{|f_{\mathrm{m},n} - f_{\mathrm{s},n}|}{f_{\mathrm{m},n}} \times 100\,, \tag{7}$$

where $f_{\mathrm{m},n}$ is the nth resonance frequency estimated from the measured data, and $f_{\mathrm{s},n}$ is the nth resonance frequency from the simulated data.

4.2.3 Damping error

Determining a frequency-domain measure of damping is challenging due to poor spectral resolution and overlapping resonance peaks. Instead of directly estimating the damping constant, we use a quantity representing it. Recognizing that modal damping correlates with a Q-factor at resonance frequencies, we evaluate and compare normalized amplitudes around these frequencies. The relative error is then

$$E_{d_\mathrm{f}} = \frac{1}{N}\sum_{n=0}^{N} \frac{\|\mathbf{a}_{\mathrm{m},n} - \mathbf{a}_{\mathrm{s},n}\|}{\|\mathbf{a}_{\mathrm{m},n}\|} \times 100\,, \tag{8}$$

where $\mathbf{a}_{\circ,n} = [a_{-k}\cdots a_0 \cdots a_k]/a_0$, are the magnitudes of the Fourier coefficients, a_0 is the magnitude at the nth resonant frequency, and k is the number of frequency bins to the left or right of the resonant frequency.

4.3 Parameter study data analysis

These measures can be used to evaluate the FEM and ISM solutions presented in the parameter study (cf. Sec. 3). Assuming that the FEM solutions are reference solutions, the ISM errors computed using the measures are presented in Tab. 1. We observe that the greatest errors occur for $E_{T_{60}}$. This agrees with the data shown in Figs. 1b, 2b, and 3b. The second largest errors appear for E_{S_f}, which can be confirmed by comparing the RTFs in Figs. 1, 2, and 3. Generally, the peaks in the RIRs and the RTFs agree.

Table 1: Error (in %) between the FEM and ISM solutions for the parameter study. For E_{S_t} and E_{p_t}, $0 \leq t \leq 0.05$ s. For $E_{T_{60}}$, $-25 \leq \mathrm{EDC} \leq -5$ dB. For E_{S_f}, E_{p_f}, and E_{d_f}, $20 \leq f \leq 100$ Hz, and $k = 1$.

	E_{S_t}	E_{p_t}	$E_{T_{60}}$	E_{S_f}	E_{p_f}	E_{d_f}
c_{-1}	1.29	0.06	7.57	4.58	0.50	0.19
c_0	1.46	0.12	12.11	5.02	0.63	0.25
c_{+1}	1.60	0.11	15.74	5.20	1.99	0.21
$0.9V$	1.58	0.04	22.19	4.98	2.24	0.24
V	1.46	0.12	12.11	5.02	0.63	0.25
$1.1V$	1.27	0.09	6.53	4.10	1.97	0.52
σ_{-1}	1.80	0.13	10.38	3.72	0.67	0.95
σ_0	1.46	0.12	12.11	5.02	0.63	0.25
σ_{+1}	0.49	0.05	21.75	0.86	0.27	0.71

4.4 Summary

The cosine similarity relative errors quantify the agreement of the features of the measured and simulated data. If these errors are large, the peak arrival time, reverberation time, resonance frequency, and damping errors can be consulted to determine which feature of the acoustic field the model does not adequately capture. Note that, since $E_{T_{60}}$ is high, E_{d_f} is lower than expected. This measure may require further development. All errors are reported in percent, making feature comparison straightforward.

5. APPLICATION OF VALIDATION MEASURES

In this section, the proposed measures are used to evaluate FEM and ISM models of an approximately shoebox-shaped room.

5.1 Experimental setup

The measured room has dimensions $9.56 \times 3.79 \times 2.54$ m^3. The speed of sound in the room is estimated to be 345 m/s, and the medium density is assumed to be 1.2 kg/m^3. The room is excited by a low-frequency loudspeaker, and omnidirectional microphones are used to capture the sound field at six positions. Estimations of the loudspeaker driver velocity and the spatially uniform, complex-valued, frequency-dependent impedance are available; for more detail, please refer to Prinn *et al.* [12].

Table 2: Measures of error (in %) between the measured data and the FEM solutions for the test case. For E_{S_t} and E_{p_t}, $0.1 \leq t \leq 0.3$ s. For $E_{T_{60}}$, $-25 \leq \mathrm{EDC} \leq -5$ dB. For E_{S_f}, E_{p_f}, and E_{d_f}, $20 \leq f \leq 100$ Hz, and $k = 1$.

	E_{S_t}	E_{p_t}	$E_{T_{60}}$	E_{S_f}	E_{p_f}	E_{d_f}
1	27.40	1.10	1.77	20.10	0.14	7.81
2	24.85	0.82	3.61	11.50	0.24	6.67
3	21.69	1.83	6.52	14.94	0.42	7.05
4	13.02	1.88	0.63	11.69	0.23	8.09
5	15.87	1.27	7.94	13.11	0.21	7.13
6	17.62	0.74	10.14	12.31	0.21	8.75

Table 3: Measures of error (in %) between the measured data and the ISM solutions for the test case. For E_{S_t} and E_{p_t}, $0.1 \leq t \leq 0.3$ s. For $E_{T_{60}}$, $-25 \leq \mathrm{EDC} \leq -5$ dB. For E_{S_f}, E_{p_f}, and E_{d_f}, $20 \leq f \leq 100$ Hz, and $k = 1$.

	E_{S_t}	E_{p_t}	$E_{T_{60}}$	E_{S_f}	E_{p_f}	E_{d_f}
1	25.76	1.07	25.62	21.21	0.31	6.62
2	23.60	0.82	24.09	12.32	0.47	8.57
3	22.07	1.83	36.16	17.00	0.40	9.55
4	11.84	1.83	18.07	9.89	0.28	6.81
5	16.59	0.49	15.51	13.60	0.32	7.53
6	17.87	7.72	16.73	12.96	0.45	9.10

5.2 Measures of validation

The measures of validation for a FEM model of the room are presented in Tab. 2, and those for an ISM model are presented in Tab. 3. We see that, in general, the FEM solutions have lower levels of error than the ISM solutions. Measures E_{p_t} and E_{p_f} indicate the speed of sound and room geometry are well captured by both models. The $E_{T_{60}}$ and E_{d_f} measures suggest that the absorption at the room's surfaces could be described more accurately.

6. CONCLUSION

This work aims to provide validation measures for users of room acoustics simulation tools. A preliminary set of measures are proposed and used to quantify errors of FEM and ISM models of a measured room. There is a margin for improvement, especially for the damping error measure, which does not satisfactorily represent the damping error. Future studies should compare these measures with existing ones, examine the effects of noise and spatial variability, and explore additional test cases.

7. REFERENCES

[1] D. M. Russel, "Error measures for comparing transient data: Part I, development of a comprehensive error measure," in *Proc. of the 68th Shock and Vibration Symposium*, 1997.

[2] L. E. Schwer, "Validation metrics for response histories: perspectives and case studies," *Eng. Comput.*, vol. 23, no. 4, pp. 295–309, 2007.

[3] C. J. Roy and W. L. Oberkampf, "A comprehensive framework for verification, validation, and uncertainty quantification in scientific computing," *Comput. Methods Appl. Mech. Eng.*, vol. 200, no. 25, pp. 2131–2144, 2011.

[4] M. Vorländer, "Computer simulations in room acoustics: Concepts and uncertainties," *J. Acoust. Soc. Am.*, vol. 133, no. 3, pp. 1203–1213, 2013.

[5] L. Aspöck, *Validation of room acoustic simulation models*. PhD thesis, RWTH Aachen University, 2020.

[6] F. Brinkmann, L. Aspöck, D. Ackermann, R. Opdam, M. Vorländer, and S. Weinzierl, "A benchmark for room acoustical simulation. concept and database," *Appl. Acoust.*, vol. 176, p. 107867, 2021.

[7] T. Thydal, F. Pind, C.-H. Jeong, and A. P. Engsig-Karup, "Experimental validation and uncertainty quantification in wave-based computational room acoustics," *Appl. Acoust.*, vol. 178, p. 107939, 2021.

[8] Y. Miki, "Acoustical properties of porous materials – modifications of delany-bazley models–," *J. Acoust. Soc. Jpn.*, vol. 11, no. 1, pp. 19–24, 1990.

[9] A. G. Prinn, "On computing impulse responses from frequency-domain finite element solutions," *J. Theor. Comput. Acoust.*, vol. 29, no. 1, p. 2050024, 2021.

[10] COMSOL multiphysics®, v. 5.5, COMSOL AB, Stockholm, Sweden.

[11] J. S. Suh and P. A. Nelson, "Measurement of transient response of rooms and comparison with geometrical acoustic models," *J. Acoust. Soc. Am.*, vol. 105, no. 4, pp. 2304–2317, 1999.

[12] A. G. Prinn, P. Panter, A. Walther, and E. A. Habets, "Validation of an eigenvalue-based inverse method for estimating locally-reacting surface impedance," *Appl. Acoust.*, vol. 228, p. 110332, 2025.